Article

The Synthesis of [(BiTe){(TiTe)}] Superlattices from Modulated Elemental Reactants

Fred R. Harris, Stacey Standridge, and David C. Johnson

J. Am. Chem. Soc., **2005**, 127 (21), 7843-7848• DOI: 10.1021/ja050799k • Publication Date (Web): 05 May 2005

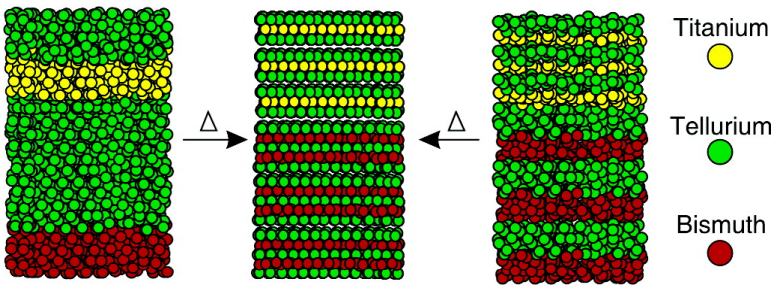

More About This Article

Additional resources and features associated with this article are available within the HTML version:

- Supporting Information
- Links to the 1 articles that cite this article, as of the time of this article download
- Access to high resolution figures
- Links to articles and content related to this article
- Copyright permission to reproduce figures and/or text from this article

View the Full Text HTML

Journal of the American Chemical Society is published by the American Chemical Society. 1155 Sixteenth Street N.W., Washington, DC 20036

J|A|C|S
ARTICLES
Published on Web 05/05/2005

The Synthesis of $[(Bi_2Te_3)_x\{(TiTe_2)_y\}_{1.36}]$ Superlattices from Modulated Elemental Reactants

Fred R. Harris, Stacey Standridge, and David C. Johnson*

Contribution from the Department of Chemistry and Materials Science Institute, University of Oregon, Eugene, Oregon 97403

Received February 7, 2005; E-mail: davej@uoregon.edu

Abstract: A solid-state growth technique is described for the preparation of misfit layered compounds $[(Bi_2Te_3)_x\{(TiTe_2)_y\}_{1.36}]$ from preconfigured reactants that provide independent control of both *x* and *y*. A procedure for optimizing the structure of the preconfigured amorphous reactants is presented demonstrating the importance of controlling both the composition and the absolute thicknesses of the component layers. Data are presented highlighting the effect of the diffusion distances of the preconfigured reactants on the kinetics of product formation.

Introduction

Over the past decades, nanostructured materials have attracted considerable attention because they offer both the ability to combine the properties of the components and create new properties dependent on the size and structure of the constituent members.[1] Tailoring properties with layered nanostructured composites has been accomplished in many areas across material science, including magnetism,[2] the design of hydrogen storage systems,[3] and semiconductors.[4] Other recent examples include thermoelectric materials in which the lowering of the thermal conductivity with the use of $[(Bi_2Te_3)_x(Sb_2Te_3)_y]$ superlattices has shown efficiencies that are more than double those of thermoelectrics made with bulk components alone.[5,6]

Techniques that typically are used to synthesize layered nanostructured materials rely on layer-by-layer deposition techniques to control surface reaction kinetics. The most developed approach is molecular beam epitaxy during which a gas-surface equilibrium is manipulated by controlling the impingement rate of the component elements and the substrate temperature which determines surface mobilities. Typically, one reactant controls the growth rate while the other is deposited in excess to compensate for its higher vapor pressure. Materials grown by molecular beam epitaxy are usually limited by the need for epitaxial relationships as well as favorable growth kinetics, but exquisitely controlled nanostructured materials are produced when optimial growth conditions are obtained.[7−9] More recently a liquid-phase deposition process has been used to create novel nanostructured materials.[10,11] In this deposition process, the substrate is alternately dipped in solutions containing different species that react in a self-limiting manner with the surface created from the previous species. This type of deposition process offers the same layer-by-layer control; however, growing at these lower temperatures causes more disorder and less structural precision because surface mobility is limited.

In this article, we describe a solid-phase growth technique from preconfigured reactants that can be used to prepare misfit layered compounds−compounds that do not have an epitaxial relationship between the constituent materials. In particular, we target the synthesis of $[(Bi_2Te_3)_x\{(TiTe_2)_y\}_{1.36}]$, where the subscript 1.36 reflects the misfit between the areas of the unit cells in the a−b plane of the constituent materials. The growth technique presented herein differs from the traditional layer-by-layer growth approaches in that the entire film is deposited as amorphous elemental layers and then ex vivo the film is annealed to form the desired and potentially metastable nanostructure. As contrasted in Figure 1, the layer-by-layer growth techniques grow the desired product directly while our approach focuses on designing the starting materials within a local minimum in free energy space containing the desired product, close enough in structure to the final product so that, upon gentle annealing, the desired kinetic structure is trapped.

Several challenges need to be overcome in the solid-phase growth technique described in this article to prepare nanostructured materials with defined structure. The first is creating the preconfigured reactants with both the composition corresponding to the stoichiometry of the component in each layer as well as depositing the exact amount of each component to form the desired number of unit cells of each component layer in the desired product. A procedure is presented for this calibration. A second challenge is determining the kinetics of the competing reactions of either phase separation or inter-

(1) Bauer, G.; Krenn, H. *Contemp. Phys.* **1991**, *32*, 383−402.
(2) Shen, J.; Kirschner, J. *Surf. Sci.* **2002**, *500*, 300−322.
(3) Seayad, A. M.; Antonelli, D. M. *Adv. Mater. (Weinheim, Ger.)* **2004**, *16*, 765−777.
(4) Patane, A.; Sherwood, D.; Eaves, L.; Fromhold, T. M.; Henini, M.; Main, P. C.; Hill, G. *Appl. Phys. Lett.* **2002**, *81*, 661−663.
(5) Venkatasubramanian, R. *Phys. Rev. B: Condens. Matter* **2000**, *61*, 3091−3097.
(6) Venkatasubramanian, R.; Slivola, E.; Colpitts, T.; O'Quinn, B. *Nature* **2001**, *413*, 597−602.
(7) Chambers, S. A. *Surf. Sci. Rep.* **2000**, *39*, 105−180.
(8) Cho, A. Y. *J. Cryst. Growth* **1991**, *111*, 1−13.
(9) Joyce, B. A.; Joyce, T. B. *J. Cryst. Growth* **2004**, *264*, 605−619.
(10) Neff, G. A.; Helfrich, M. R.; Clifton, M. C.; Page, C. J. *Chem. Mater.* **2000**, *12*, 2363−2371.
(11) Woodall, J. M. *J. Cryst. Growth* **1972**, *12*, 32−38.

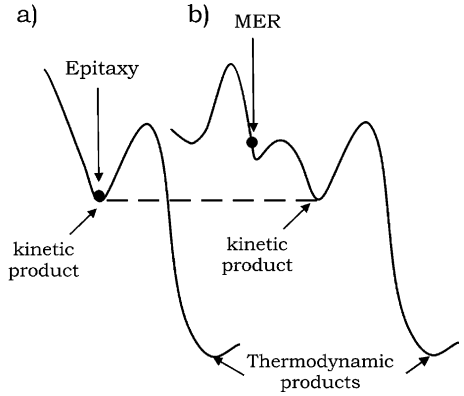

Figure 1. (a) Epitaxy grows the kinetic metastable material in a kinetic well. (b) Modulated elemental reactants are used to control the starting point on the reaction surface diagram. By controlling this starting point, metastable products can form by annealing the samples at low temperatures (usually <500 °C). This supplies enough energy to fall into the kinetic energy well without continuing to the thermodynamically well.

diffusion (if the components are immiscible or miscible, respectively) versus the self-assembly that occurs during crystallization of the desired product. We compare reaction kinetics of two reactant precursors with different diffusion lengths showing the dependence of reaction rate on the extent of preorganization in the initial reactant. We demonstrate the ability of this approach to prepare mismatched layered nanostructured materials with unit cell control of the final structure.

Experimental Section

Multilayer elemental precursors were deposited in a cryopumped high vacuum (<5×10^{-7} Torr) deposition chamber. A Thermionics electron beam gun was used to evaporate titanium, while Applied Epi-Veeco SUMO effusion cells were used to evaporate bismuth and tellurium. Within each effusion cell, a boron nitride crucible contained the element to be deposited. There are two separate heaters that control the top and bottom of the cell independently. One surrounds the top one-third of the BN crucible, and the other surrounds the bottom two-thirds of the BN crucible. The temperature of the tellurium cell was controlled by only supplying current to the top heater to an approximate temperature of 550 °C to give a deposition rate at the sample of approximately 0.4 Å/s. The bismuth cell was heated with both heaters. The top was kept at approximately 800 °C, while the bottom was kept at approximately 500 °C. The bottom heater was adjusted in power to give the approximate deposition rate at the sample of 0.4 Å/s. For all of the sources, the measured rate was determined from quartz microbalances (QMB) placed 10 in. above each evaporation source. Six-inch silicon substrates were placed 30 in. above each source and were coated with poly(methyl methacrylate), which could be dissolved later for removal of the deposited film. To this, an uncoated piece of polished silicon was attached for X-ray reflectivity (XRR) and X-ray diffraction (XRD) studies. All measured rates were determined at a 100% tooling ratio (i.e., the deposition rate on the sample substrate is assumed to be the same as the deposition rate as on the QMB). Actual deposition thicknesses were determined experimentally as reported in the subsequent section.

Pneumatic shutters, timed with a personal computer, were used to control which source deposited on the substrate. When performing a deposition, each effusion cell source was brought to the approximate measured rate mentioned above, and then a time-averaged rate was determined every minute until the rate was stable. The time-averaged rate was assumed to be constant during the experimental run. For electron beam gun deposition, a feedback loop from the QMB controlled the power delivered to the gun.

XRR was used to determine thicknesses of the $[(Bi_2Te_3)_x\{(TiTe_2)_y\}_{1.36}]$ solid-state precursors and was used as a probe during the evolution of the precursor with annealing. XRD was also used in the structure determination of the final product after annealing in an N_2 environment (<0.5 ppm oxygen). Rocking curve data were collected during the various stages of formation to indicate the degree of crystallographic alignment of the evolving crystal structure with the substrate. In a rocking curve measurement, the incident and exit angles of the diffractometer are set at the Bragg condition, and the sample stage is rotated to positive and negative angles within the diffraction plane. Crystallographically aligned samples have a maximum at zero stage rotation, and the full width at half-maximum (fwhm) describes the range of crystallite orientation relative to the substrate. Randomly oriented samples would show a constant intensity as a function of stage rotation. These studies were performed on a Bruker D8 Discover X-ray diffractometer, which used a fixed Cu Kα (1.54 Å) radiation source, while the sample and detector were moved to achieve the desired Bragg geometry. Samples were step-annealed in a box furnace to different temperatures in a N_2 atmosphere (<0.5 ppm O_2) for structural studies as a function of annealing temperature and time.

Electron probe microanalysis (EPMA) was used in a wavelength dispersive mode to obtain the composition of the initial binary components so that their thickness ratios could be calibrated as described below. The films on a silicon substrate were analyzed using three different accelerating voltages (5, 15, and 20kV), which were used to model the composition with a known thickness from XRR using Stratagem modeling software (version 3.0).

Results

In the creation of the nanostructured precursors of $[(Bi_2Te_3)_x\{(TiTe_2)_y\}_{1.36}]$, both composition and the absolute amounts of each block of the precursor are crucial and need to be controlled. This can be challenging because factors such as sticking coefficients, monitored versus actual thickness, and the densities of the deposited layers are unknown and can vary as surfaces and layer thicknesses change. A total of 14 samples were deposited to calibrate the ratio of the elemental layer thicknesses required to obtain the compositions for the desired binary materials Bi_2Te_3 and $TiTe_2$ (see Table 1). For each binary system, a series of samples were deposited in which the tellurium thickness was held constant and either bismuth or titanium was varied, as illustrated in Figure 2a. Composition was measured with EPMA, and the ratio of QMB thicknesses that produced compositions corresponding to the desired Bi_2Te_3 and $TiTe_2$ compositions was determined by regression.[12] It was then assumed that this ratio between the amorphous elemental layers would be scalable to any desired thickness while maintaining the desired composition.

Once the thickness ratios required to produce the desired compositions in each of the binary systems were determined, the next challenge was to calibrate the absolute amount of each of the components required to form the targeted $[(Bi_2Te_3)_3\{(TiTe_2)_3\}_{1.36}]$ compound. To determine the absolute amount of bismuth and tellurium that resulted in three [Te−Bi−Te−Bi−Te] layers (30 Å) of bismuth telluride and the absolute amount of material of titanium and tellurium that resulted in three [Te−Ti−Te] layers of titanium telluride (19.5 Å)[13,14] during one deposition cycle, Ti−Te and Bi−Te layers were sequentially deposited to prepare layered nanostructured precur-

(12) Jensen, J. M. *Chemistry*; University of Oregon: Eugene, OR, 2003.
(13) Stordeur, M. In *CRC Handbook of Thermoelectrics*; Rowe, D. M., Ed.; CRC Press: Boca Raton, FL, 1995; pp 239−255.
(14) Arnaud, Y.; Chevreton, M. *J. Solid State Chem.* **1981**, *39*, 230−239.

Table 1. Data Used To Determine the Relationship between the Ratio of QMB Thicknesses and the Atomic Composition[a]

sample No.	bismuth QMB thickness (arb Å)	titanium QMB thickness (arb Å)	tellurium QMB thickness (arb Å)	atomic % Bi	atomic % Ti
A1	6.7	–	16.0	28	–
A2	8.3	–	16.0	34	–
A3	10.0	–	16.0	38	–
A4	12.7	–	16.0	42	–
A5	13.3	–	16.0	44	–
A6	15.0	–	16.0	47	–
A7	16.7	–	16.0	49	–
A8	18.3	–	16.0	51	–
A9	20.0	–	16.0	54	–
A10	–	5.0	16.0	–	22
A11	–	6.7	16.0	–	29
A12	–	8.3	16.0	–	35
A13	–	10.0	16.0	–	43
A14	–	11.7	16.0	–	53

[a] Uncertainties in measured QMB thicknesses are on the order of 0.1, while compositions determined in using electron probe microanalysis have uncertainties on the order of 1 atomic %. The arb Å thicknesses are calculated assuming a tooling factor of 1.00 as described in the text.

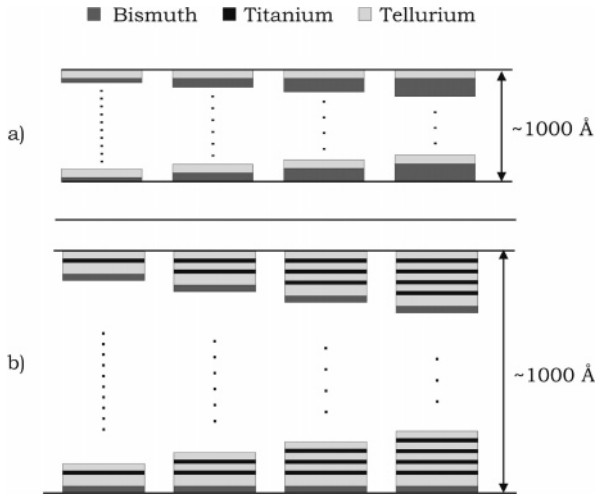

Figure 2. Schematic of misfit layered precursor calibration. (a) Atomic ratios are calibrated for composition by varying either the bismuth or titanium layer thickness while holding the thickness of the tellurium layer constant. (b) Samples are made for absolute amount calibration by depositing a series of samples varying the number of times the Ti−Te layers are deposited, while keeping the number of Bi−Te layers constant.

sors. Four series consisting of a total of 13 samples were prepared (see Table 2). Samples were deposited in which the number of Bi−Te layers deposited was held constant while the number of Ti−Te layers was systematically increased as illustrated in Figure 2b (i.e., one set of Ti−Te layers was deposited in the repeating unit for one sample, while the next sample had two sets of Ti−Te layers in the repeating unit, three sets for the next, and so on). The resulting systematic change in total thickness of the repeating unit, determined from XRR data, allowed the actual thicknesses for each layer to be extrapolated for each of the four series (Figure 3). The total thickness of each component was adjusted between each set of samples so that the layer thicknesses for each binary phase approached the thickness calculated from the *c* lattice parameters reported in the literature for each of the components. Experiments leading up to this calibration showed little contraction of the amorphous precursors during crystallization, and thus it was possible to use the thicknesses calculated from the binary compounds as targets for the deposition process. More typically significant contraction of deposited layers is observed during crystallization and would need to be factored into the targeted thickness of the deposited layers.

The total amount of each component deposited is critical to the crystal quality of the resulting product. Having too much or too little material dramatically affects the ability of the precursor to self-organize into the desired compound, as excess material needs to diffuse out to the grain boundaries to permit the formation of the desired layered structure. To illustrate the importance of the absolute amount calibration sequence, Figure 4 shows a comparison of XRD patterns of samples B1, B5, B8, and B12, which were targeted to form $[(Bi_2Te_3)_3\{(TiTe_2)_3\}_{1.36}]$ (from Table 2) after being annealed for 30 min at 280 °C in a N_2 environment. In sample B1, which was several Ångstroms from the targeted layer thicknesses of each component, only broad weak high-order diffraction maxima are observed, suggesting little long-range crystallographic alignment of the two component layers with one another. As the thicknesses of the component layers are calibrated closer to the exact amounts needed to make the $[(Bi_2Te_3)_3\{(TiTe_2)_3\}_{1.36}]$ misfit layered compound (samples B5 and B8), the high-order Bragg reflections become more prominent. Sample B12 is taken to be the closest to the correct absolute amounts due to both the higher intensity of the higher-order diffraction peaks and the larger number of diffraction maxima observed. The diffraction lines are broadened by the small number of unit cells in the sample (20), total film thickness (~1000 Å), and a potentially high concentration of defects resulting from the low-temperature synthesis technique.

The diffraction patterns shown in Figure 4 can all be indexed based on a one-dimensional unit cell expected for a film with preferred crystallographic alignment. Rietveld analysis of the diffraction pattern of sample B12 was undertaken to obtain more information about the structure of $[(Bi_2Te_3)_3\{(TiTe_2)_3\}_{1.36}]$ perpendicular to the substrate. Bulk Bi_2Te_3 crystallizes in the $R\bar{3}m$ space group, while bulk $TiTe_2$ crystallizes in the $P\bar{3}m1$ space group. The $[(Bi_2Te_3)_x\{(TiTe_2)_y\}_{1.36}]$ system was refined with the general structure analysis system[15,16] in the $P\bar{3}m1$ space group, although a definitive space group cannot be assigned because only 00*l* reflections are observed. The atomic occupancy within the $TiTe_2$ layer was allowed to refine with a higher than

(15) Larson, A. C.; Dreele, R. B. V. *GSAS (General Structure Analysis System)*; Report LA-UR-86-748; Los Alamos National Laboratory: Los Alamos, NM, 2000.
(16) Toby, B. H. *J. Appl. Crystallogr.* **2001**, *34*, 210−213.

Table 2. Summary of the Samples Used To Determine the Tooling Factors between the QMB Thickness and the XRR Determined Thickness of Each Component Layer

	superlattice precursor										
	Bi–Te layers (Bi_2Te_3 component)			Ti–Te layers ($TiTe_2$ component)			XRR	regression		tooling factor	
sample ID	bismuth QMB thickness[a]	tellurium QMB thickness[a]	No. of repeats	titanium QMB thickness[a]	tellurium QMB thickness[a]	No. of repeats	measured total layer thickness[b]	Bi–Te thickness[b]	Ti–Te thickness[b]	Bi–Te tooling factor[c]	Ti–Te tooling factor[c]
B1	42.1	61.2	1	19.8	46.0	1	42.7	26.8	15.8	25.9	24.0
B2	42.1	61.2	1	19.8	46.0	2	58.0	26.8	31.6	25.9	24.0
B3	42.1	61.2	1	19.8	46.0	3	74.3	26.8	47.3	25.9	24.0
B4	42.1	61.2	1	19.8	46.0	4	89.9	26.8	63.1	25.9	24.0
B5	43.6	63.4	1	28.0	65.0	1	53.3	31.7	21.9	29.7	23.6
B6	43.6	63.4	1	28.0	65.0	2	76.4	31.7	43.9	29.7	23.6
B7	43.6	63.4	1	28.0	65.0	3	97.1	31.7	65.8	29.7	23.6
B8	42.9	62.3	1	24.1	56.1	1	51.0	30.5	20.3	29.0	25.3
B9	42.9	62.3	1	24.1	56.1	2	70.8	30.5	40.6	29.0	25.3
B10	42.9	62.3	1	24.1	56.1	3	91.5	30.5	60.9	29.0	25.3
B11	42.9	62.3	1	24.1	56.1	4	111.7	30.5	81.2	29.0	25.3
B12	43.7	63.6	1	23.3	54.2	1	51.2	31.8	19.4	29.7	25.1
B13	43.7	63.6	1	23.3	54.2	2	70.7	31.8	38.8	29.7	25.1

[a] In arb Å. [b] In Å. [c] In percent.

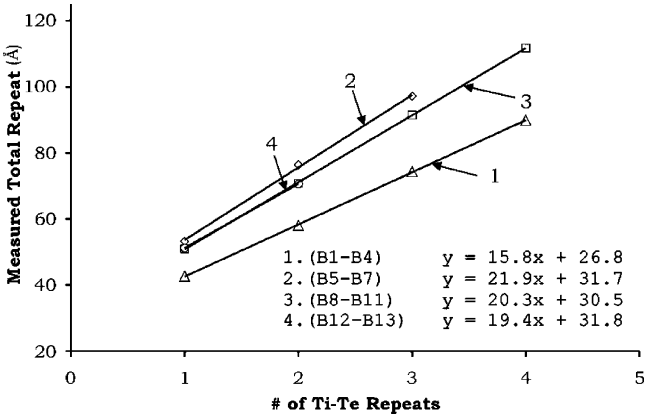

Figure 3. Plot of the measured repeat spacings as a function of the varied Ti−Te thickness. The equations of the regressed lines show the Bi−Te thicknesses (*y*-intercept) and Ti−Te thicknesses (slope) determined for each set of runs.

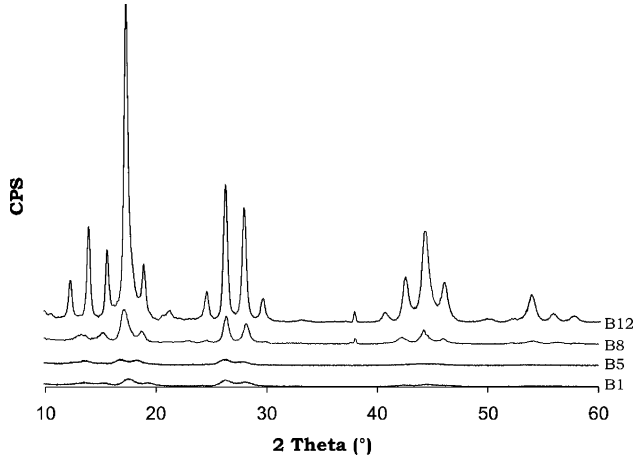

Figure 4. X-ray diffraction patterns of annealed preconfigured reactants during the absolute amount calibration.

100% occupancy because of the large mismatch in *a* lattice parameters of the two component layers. The results of the refinement are summarized in Figure 5. The $TiTe_2$ layer was refined to be 36% more atomically dense than the Bi_2Te_3 layer, indicating that the atomic densities of the component layers are close to the atomic densities of the bulk compounds. The layer

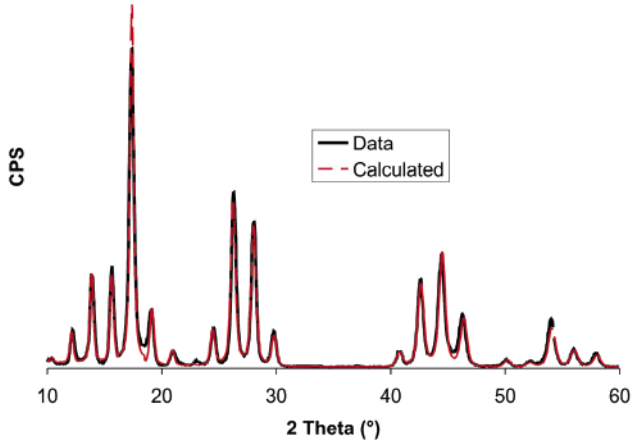

Atom	x	y	z	Fraction	Symmetry Position
TE1	0	0	0.000	0.93	1a
BI2	0	0	0.041	1.00	2c
TE3	0	0	0.075	1.00	2c
TE4	0	0	0.125	1.00	2c
BI5	0	0	0.160	1.00	2c
TE6	0	0	0.201	1.00	2c
BI7	0	0	0.241	0.97	2c
TE8	0	0	0.274	1.00	2c
TE9	0	0	0.338	1.36	2c
TI10	0	0	0.370	1.36	2c
TE11	0	0	0.406	1.36	2c
TE12	0	0	0.467	1.36	2c
TI13	0	0	0.500	1.36	1b

c = 50.65 χ^2 = 40.06 xRp = 0.2688 Rp = 0.2097

Figure 5. Rietveld analysis of $[(Bi_2Te_3)_3\{(TiTe_2)_3\}_{1.36}]$ refined in the $P\bar{3}m1$ space group. Uncertainties in fractional occupancies are on the order of 0.01 and uncertainties in the *z*-coordinates of the atoms are on the order of 0.001.

spacings between the atomic layers within the Bi_2Te_3 layer resemble bulk Bi_2Te_3, and the layer spacings within the $TiTe_2$ layer resemble bulk $TiTe_2$. The van der Waals gap (VWG) between the two component layers resembles the spacing of the VWG in bulk $TiTe_2$ layers.

The diffraction data collected as a function of the absolute amount of Ti/Te and Bi/Te deposited in each repeating unit

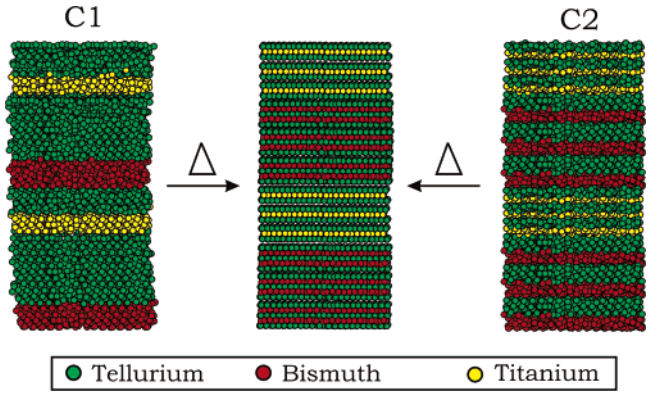

Figure 6. Idealized representations of the two different preconfigured reactants leading to $[(Bi_2Te_3)_3\{(TiTe_2)_3\}_{1.36}]$. C1 repeats once for every three layers of Bi_2Te_3 or $TiTe_2$ and has the longest diffusion distance. C2 repeats once for every layer of Bi_2Te_3 or $TiTe_2$ and consequently has a much shorter diffusion distance.

coupled with the structural information obtained from Rietveld analysis indicate that for this family of misfit layered compounds x and y must be integers in the general formula $[(Bi_2Te_3)_x\{(TiTe_2)_y\}_{1.36}]$. The calibration procedure described above can be used to prepare members of this family where x and y are divisible by 3. To gain access to all possible integers x and y, the calibration procedure needed to be repeated targeting the case where the sequential deposition of the component elements yields the correct amount of material to give one layer of each the component binary compounds (Te−Bi−Te−Bi−Te or Te−Ti−Te). Rather than repeat the entire calibration procedure, we divided the deposition times determined above by 3 as a starting point for this new calibration. Slight adjustments to the absolute amount of each component layer were made to optimize the resulting diffraction patterns of the annealed samples. These corrections were most likely needed because of the slight difference in sticking coefficients resulting from the higher number of interfaces.

The two calibrations enabled us to prepare two different elementally modulated reactants with different diffusion lengths that should both form the same $[(Bi_2Te_3)_3\{(TiTe_2)_3\}_{1.36}]$ misfit layered compound as shown in Figure 6. The sample made with one repeat for every three layers (Sample C1) gives the largest diffusion length possible in each component layer for this specific misfit layered compound, while the sample made with one repeat for every layer (Sample C2) results in a very short diffusion length. To determine the effect of diffusion distance on the reaction kinetics involved in forming the desired misfit layered compound, diffraction data were collected as a function of reaction time and temperature as shown in Figure 7.

In sample C1, the longer diffusion length case, crystallites from both component layers have begun to form on deposit as determined by the weak broad diffraction maxima that is seen around areas of the diffraction pattern associated with Bi_2Te_3 and $TiTe_2$. As the samples are annealed, the layers continue interdiffusion and the crystallites grow larger. At approximately 150 °C, the broad diffuse peaks in the XRD begin splitting. This splitting indicates that long-range order is occurring between the components in different repeating units. Between 150 and 200 °C, the intensity of the split peaks in the XRD continue to grow. The fwhm of the rocking curves around 13.9° (008) and 17.4° (00 10), which show the degree of orientation

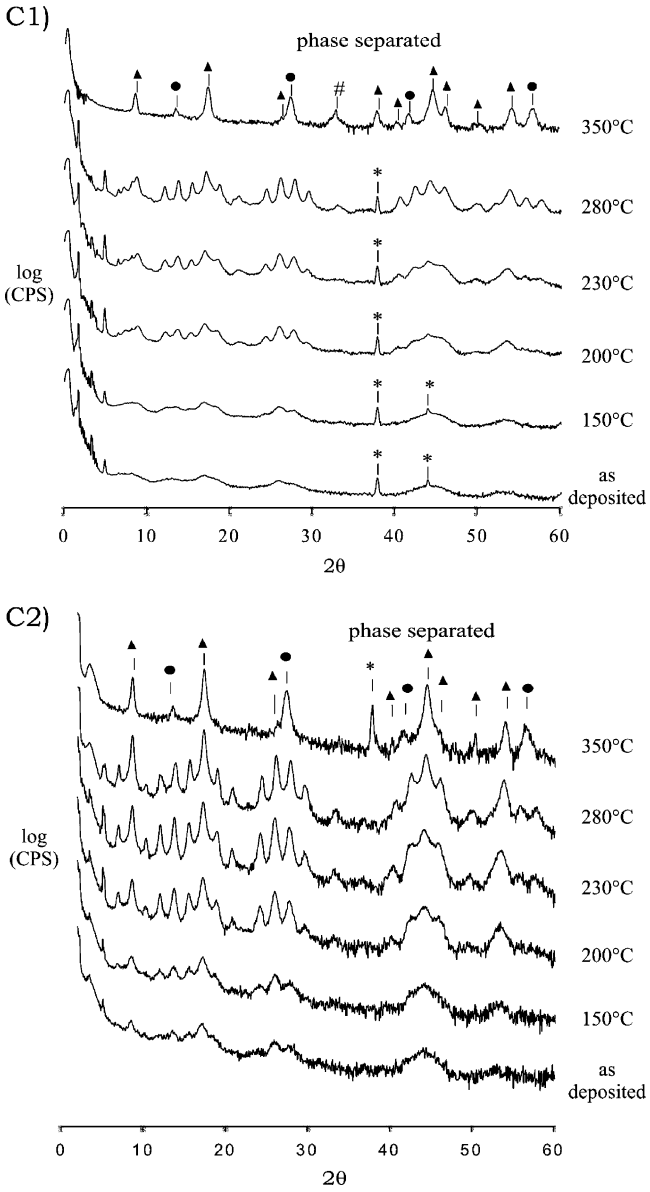

Figure 7. XRD as a function of annealing temperature in the $[(Bi_2Te_3)_3\{(TiTe_2)_3\}_{1.36}]$ misfit layered compound. (*) indicates peaks from the sample holder, and (#) indicates substrate peaks. In the phase-separated material, (●) and (▲) indicate peaks from Bi_2Te_3 and $TiTe_2$, respectively.

of the crystallites in the $TiTe_2$ and the Bi_2Te_3 component layers, respectively, become more aligned with the substrate (Figure 8). From 230 to 280 °C, the peaks in the XRD continue to grow in intensity, and the component layers continue to align to the substrate to a minimum fwhm of 3.2°. During this temperature range, the roughness, as determined from intensity of diffuse scattering observed in the rocking curve scans around the (001) Bragg reflection, increases steadily. This suggests that, during this period, crystal growth occurs from an Ostwald ripening process in which the larger, more aligned crystals devour the smaller, less aligned crystallites. Temperatures above 300 °C causes $[(Bi_2Te_3)_3\{(TiTe_2)_3\}_{1.36}]$ to phase-separate into their constituent components of Bi_2Te_3 and $TiTe_2$.

In sample C2, the shorter diffusion length case, the XRD of the as-deposited sample has more intense and more clearly resolved higher-order Bragg reflections than did the XRD of the as-deposited C1 sample, indicating that more long-range

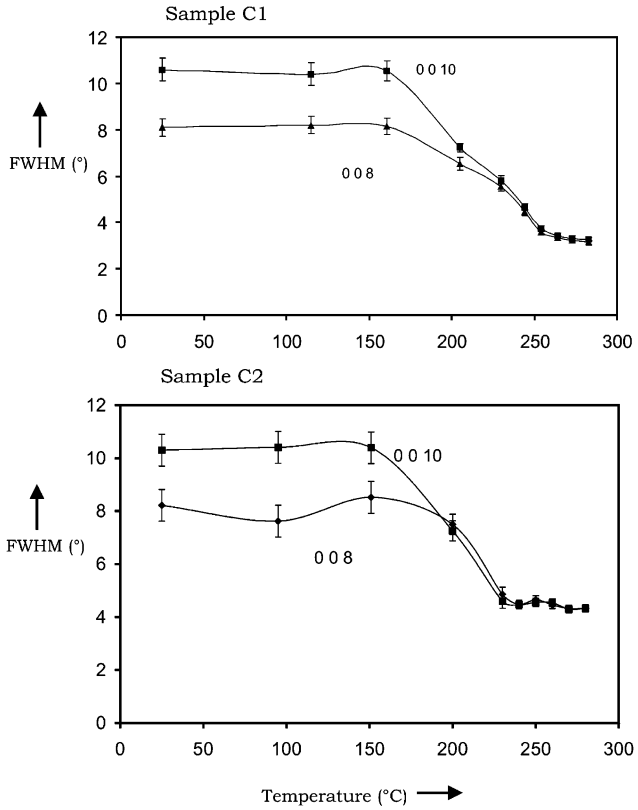

Figure 8. Comparison of the fwhm of the rocking curves around the (008) and the (00 10) between samples C1 and C2.

order between component layers in the system exists on deposit. The alignment of the (008) and the (00 10) peaks as indicated by rocking curve analysis of sample C2 show the same distribution of crystallite orientations (8° for the (008) reflection and 10° for the (00 10) reflection) as found in sample C1. At 200 °C, the superlattice diffraction peaks in sample C2 are much more distinct and intense compared to the diffraction data of sample C1. Subsequent annealing only marginally improves the spectrum obtained after annealing at 200 °C, indicating that the shorter diffusion distance case requires less energy and time to form $[(Bi_2Te_3)_3\{(TiTe_2)_3\}_{1.36}]$ than the longer diffusion distance case. The rocking curve width of the (008) and (00 10) Bragg reflections stops changing at 230 °C, reaching a minimum of about 4.2°. By 240 °C, the roughness determined by the diffuse scattering around the (001) peak has reached a maximum. No further structural changes are observed in the diffraction scans until phase separation occurs at around 300 °C.

The differences between the rates of the formation of $[(Bi_2Te_3)_3\{(TiTe_2)_3\}_{1.36}]$ in samples C1 and C2 reflect the different diffusion distances. The preconfigured reactant associated with sample C2 has shorter diffusion lengths and could be considered closer to the structure of the desired $[(Bi_2Te_3)_3\{(TiTe_2)_3\}_{1.36}]$ misfit layered compound than reactant C1. Thus, the energy and time required for sample C2 to reach the final product are less. The larger degree of misalignment of the crystallites in sample C2 as compared to that of sample C1 can perhaps be attributed to larger crystals forming in the sample at lower temperature, reducing the driving force for an Ostwald ripening process.

Conclusions

Solid-phase growth offers a controlled route to the formation of misfit layered compounds with control over the thickness of each of the components. This synthesis technique places the focus on controlling the structure of a preconfigured reactant rather than controlling the surface kinetics of a layer-by-layer growth technique. A procedure was presented to calibrate the structure of preconfigured reactants to produce the desired $[(Bi_2Te_3)_x\{(TiTe_2)_y\}_{1.36}]$ misfit layered compound with defined integer values of x and y. In these preconfigured reactants, diffusion lengths are important in controlling the kinetics of product formation. Shorter diffusion lengths result in more facile formation of the desired misfit layered compound.

Acknowledgment. This work was supported by the National Science Foundation (DGE 0114419, DMR 9813726, and DMR 0103409) and the Office of Naval Research (ONR N00014-04-1-0407).

JA050799K